

Four-wave mixing instabilities in tapered and photonic crystal fibers

F. Biancalana, D.V. Skryabin, and A. Ortigosa-Blanch

*Department of Physics, University of Bath
Bath BA2 7AY, United Kingdom*

December 9, 2018

Abstract

We present an analytical study of four-wave mixing instabilities in tapered fibers and photonic crystal fibers. Our approach avoids the use of Taylor expansion for the linear susceptibility and the slowly-varying envelope approximation. This allows us to describe the generation of sidebands strongly detuned from the pump wave with simultaneous account for the entire dispersion characteristic of a fiber, which is found to be important for describing properly the key role of the parametric instabilities in the supercontinuum generation in these kind of fibers.

OCIS code: 060.4370, 190.2620

INTRODUCTION

Four-wave mixing (FWM) is one of the most fundamental processes in optics, consisting in the generation of a pair of Stokes and anti-Stokes photons out of two strong pump photons [1, 2]. FWM can be observed in a wide range of materials with Kerr nonlinearity including optical fibers [3]. The efficiency of FWM (which is a coherent process) strongly depends on the so-called phase matching conditions imposed on the wave-vectors of the pump and generated waves [3]. In a conventional single-cladding optical waveguide, the phase matching conditions are satisfied only in the vicinity of the zero-dispersion point, as it has been demonstrated for dispersion-shifted fibers

and for standard telecommunication fibers [4, 5], even if there are several techniques (for example using modal birefringence) which can extend the phase-matched frequency-range [6].

Several experimental results on observation of four-wave mixing in photonic crystal fibers (PCFs) [7] and tapered fibers (TFs) [8] have been published over the last several years [9, 10, 11]. These relatively new kind of fibers represent an ideal system for investigating the optical nonlinearities in fused-silica, because of their unique dispersive and nonlinear properties (see for example [12, 13]). In particular, the enhanced nonlinearity due to the smallness of the effective core area can increase dramatically every nonlinear effect.

The phase matching conditions for these fibers are found to be quantitatively different with respect to ordinary fibers: phase matching in PCFs and TFs can be achieved for a long range of pump wavelengths, because the strong waveguide contribution to the overall dispersion permits a compensation of the material dispersion for a broad window of frequencies. On the other hand, the improved nonlinearity can generate a nonlinear coefficient which can further improve the compensation in the phase.

Moreover, the dispersion characteristics of TFs [8] can be very similar to the ones found in PCFs. This is because in a typical index-guiding PCF most of the light is guided in the tiny silica core surrounded by a periodic structure of large air filled holes separated by thin membranes, which makes it very similar to TFs with guiding due to total internal reflection at the interface between silica and air [8], and in fact the eigenvalue equation used to find the group velocity dispersion (GVD) in TFs can describe with a good approximation the propagation of light in PCFs as well [14], provided that we substitute the complex cladding structure of PCF with an effective refractive index [15]. Thus, because of the fact that the GVD profile is qualitatively similar in these fibers, they can have analogous properties in the dynamical behavior of light propagation, as we shall see in the following.

Fig. 1 shows numerically calculated examples of the frequency dependence of the dispersion parameter $D = -(2\pi\omega^2/c)\partial_\omega^2\beta$, where β is the propagation constant of the fundamental mode [3], for a PCF with an elliptical core surrounded by 4 periods of air holes with an average diameter of $0.84 \mu\text{m}$ and a pitch of $\Lambda = 1.46 \mu\text{m}$, and a TF with $1 \mu\text{m}$ of core diameter, used in recent experiments on solitonic fission and supercontinuum generation (SCG) carried out by our group [8, 16, 17]. Both dispersion characteristics show two zero dispersion (ZD) points limiting a central region of anomalous group

velocity dispersion (GVD), which is a typical situation for these fibers.

In several important studies FWM in PCFs has been identified as one of the primary mechanisms contributing to generation of optical supercontinuum by ultrashort pulse propagation, at least in the first stage of the spatial propagation [9, 10, 18].

However, the analytical calculations complementing these results were either based on the standard analysis of some improved versions of the nonlinear Schroedinger equations (NLSE) [19] or on the direct analysis of the phase matching conditions [9, 10, 11, 20].

In this paper we investigate theoretically the role of parametric instabilities in PCFs and TFs, and we establish a deep link between these instabilities and the broad spectrum obtained in SCG, stimulated by recent experimental works ([9, 10]) in which the primary mechanism of spectral broadening is identified as the combined action of stimulated Raman scattering and parametric FWM. We shall find out that the unusual GVD profile of these kind of fibers will play a key role in determining the instability regions, and the analysis of these instabilities cannot be rigorously treated with a Taylor expansion around the carrier frequency of the pulse because of its flatness and curvature. Moreover, we propose a mechanism for exciting a broad window of frequencies, based on the merging between different instability regions.

MODEL EQUATION AND STABILITY ANALYSIS

The formal mathematical approach to the FWM problem is to study the stability of the strong pump wave in the presence of weak perturbations with different frequencies. The typical instability of the pump wave occurring in optical fibers is the so-called modulation instability (MI) [3], which is a particular case of the more general phenomenon of parametric FWM. More specifically, MI can be interpreted as a four-photon process driven by the self-phase modulation (SPM), and it is a general feature of wave propagation in dispersive nonlinear media. In optical fibers MI is due to the conservative interaction between nonlinearity and linear dispersion, which leads to a modulation of amplitude and phase of a continuous wave (CW) in presence of quantum noise or any other weak perturbation. Traditionally the theoretical approach to describe MI in fibers is performed using the nonlinear Schroedinger equation, that is the simplest equation which takes into account the interplay between dispersion and nonlinearity. NLSE in the context of fiber optics is derived from Maxwell's equations under the assumption

of the weakly-guiding weakly-nonlinear approximations and using a reductive perturbation procedure consisting of the spatio-temporal slowly-varying envelope approximation (SVEA) and Taylor expansion of the linear susceptibility: $\chi^{(1)}$ [3]. The expansion of the latter is often done up to second order, which corresponds to the quadratic frequency dependence of the mode propagation constant β : $\beta \sim \omega^2$. If GVD at the carrier frequency ω is relatively small, then higher order terms in the expansion of $\chi^{(1)}$ become relevant to describe propagation of waves in fibers in general and MI in particular, see e.g. [21].

However, for some fibers with complex dispersion profile and/or in cases, when FWM results in generation of frequencies far detuned from the pump, the NLSE-based approach and in particular the Taylor expansion for $\chi^{(1)}$ become inapplicable and new approaches have to be developed. One of them is to introduce a system of coupled NLSEs for pump, Stokes and anti-Stokes waves [3].

Another more sophisticated method is to avoid the Taylor expansion of $\chi^{(1)}$ and analyze the frequency mixing using a single equation, see [22] and [23]. In [22] this was mainly done in order to analyze the influence of the Raman effect on MI, and in [23] it was applied to describe FWM in dispersion-flattened fibers. Our goal here is to further develop the theories reported in [22, 23] and consider PCFs and TFs as examples, thereby providing a theoretical underpinning for recent experimental results [9, 10, 11, 19].

We begin our analysis from the nonlinear wave equation derived directly from Maxwell's equations:

$$\nabla^2 \mathbf{E} - \nabla(\nabla \cdot \mathbf{E}) - \frac{1}{c^2} \partial_t^2 (\mathbf{E} - \mathbf{P}_L - \mathbf{P}_{NL}) = 0, \quad (1)$$

where the linear polarization is defined as

$$\mathbf{P}_L = \int \chi^{(1)}(t - t', x, y) \mathbf{E}(t') dt'. \quad (2)$$

\mathbf{E} is the electric field, and $\chi^{(1)}$ is the linear susceptibility of the dielectric medium (in our case silica glass), which depends on time and the transverse coordinates x, y . \mathbf{P}_{NL} is assumed to have a simple Kerr form: $\mathbf{P}_{NL} = \chi_3 |\mathbf{E}|^2 \mathbf{E}$. Even though the Raman effect (i.e., a delayed response of the nonlinear susceptibility) can be incorporated into the theory developed below, analysis of details of its influence on FWM is well known and goes beyond the objectives of this paper [22, 24].

Our next step is to reduce Eq. (1) to an equation in z and t only. In order to achieve this we first transform Eq. (1) from time to frequency domain, using Fourier transform \mathcal{F} , and then separate transverse and longitudinal degrees of freedom through the approximate factorization

$$\mathcal{F}\mathbf{E}(x, y, z, t) = \hat{\mathbf{E}}(x, y, z, \omega) \simeq \mathbf{F}(x, y, \omega) \tilde{E}(z, \omega). \quad (3)$$

\mathbf{F} is the fundamental eigenmode of the linear waveguide having propagation constant $\beta(\omega)$. $\beta(\omega)$ incorporates both material and waveguide contributions into the overall fiber dispersion. The factorization becomes possible due to the weakness of the energy transfer from the fundamental mode to the higher order modes [25, 26].

It can be shown that after using Eq. (3) the dynamics of the inverse Fourier transform $\mathcal{F}^{-1}\tilde{E} = \bar{E}(z, t)$ of the amplitude \tilde{E} is governed by the equation

$$c^2 \partial_z^2 \bar{E} - \partial_t^2 \bar{E} = \partial_t^2 \left[\int_{-\infty}^t \chi_{eff}^{(1)}(t-t') \bar{E}(t') dt' + \bar{\chi}_3 |\bar{E}|^2 \bar{E} \right], \quad (4)$$

where $\chi_{eff}^{(1)}$ is an effective linear susceptibility of the fiber, with its Fourier transform given by

$$\hat{\chi}_{eff}^{(1)}(\omega) = \mathcal{F}\chi_{eff}^{(1)} = \beta^2 c^2 / \omega^2 - 1 \quad (5)$$

and

$$\bar{\chi}_3 = \frac{\int |\mathbf{F}|^4 dS}{\int |\mathbf{F}|^2 dS} \chi_3, \quad (6)$$

where S is the fiber area [14]. $\bar{\chi}_3$, with good accuracy, can be considered as a frequency independent coefficient, which follows from the weak frequency dependence of \mathbf{F} and χ_3 [3].

Thus we have derived a version of the wave-equation with delayed linear and instantaneous nonlinear responses. Note that Eq. (4) is an equation for the field, and not for the envelope. Expanding $\hat{\chi}_{eff}^{(1)}$ into Taylor series for small frequency detunings and making standard SVEA (in space and in time), one can easily reduce (4) to the conventional NLSE.

We assume now that our fiber is pumped by a monochromatic continuous wave (CW)

$$\bar{E} = E_0 e^{i(kz - \omega t)} + c.c., \quad (7)$$

where E_0 is a constant amplitude, k and ω are the wave-number and the frequency of the pump wave. It is easy to see that Eq. (7) solves Eq. (4) and represents a steady-state solution, provided that the following dispersion relation is satisfied:

$$k^2(\omega, |E_0|^2) = \frac{\omega^2}{c^2} \left[1 + \hat{\chi}_{eff}^{(1)}(\omega) + \bar{\chi}_3 |E_0|^2 \right]. \quad (8)$$

To find the frequencies generated within the fiber as a result of the destabilization of the pump wave, we perturb solution (7) with small complex perturbations $\epsilon(z, t)$:

$$E = [E_0 + \epsilon(z, t)] e^{i(kz - \omega t)} + c.c. \quad (9)$$

After substitution of (9) into the governing equation (4) we disregard all the terms nonlinear in ϵ . Then we assume that the complex perturbation has the following simple form, which excite both the Stokes and the anti-Stokes bands:

$$\epsilon(t) = A \exp(i\kappa z - i\delta t) + B^* \exp(-i\kappa^* z + i\delta t), \quad (10)$$

and derive a linear eigenvalue problem for the vector $(A, B)^T$ with an eigenvalue κ . It is possible to prove that the solvability condition for A and B requires that the following fourth-order polynomial equation in κ is satisfied:

$$\begin{aligned} \kappa^4 - (k_+^2 + k_-^2 + 2k^2)\kappa^2 + 2k(k_+^2 - k_-^2)\kappa \\ + (k_+^2 - k^2)(k_-^2 - k^2) - \frac{\bar{\chi}_3^2}{c^4} E_0^4 (\omega + \delta)^2 (\omega - \delta)^2 = 0, \end{aligned} \quad (11)$$

where k_{\pm} are the effective wave numbers of the Stokes and anti-Stokes waves, which include nonlinear corrections: $k_{\pm} \equiv k(\omega \pm \delta, 2|E_0|^2)$.

Solution (7) becomes unstable provided that Eq. (11) has at least one root such that $Im(\kappa) < 0$. As usual, the instability gain is given by

$$g(\delta) \equiv 2|Im(\kappa)|. \quad (12)$$

In the next section we explore the numerical solutions of Eq. (11).

FOUR-WAVE MIXING INSTABILITIES

We have scanned numerically the dependence of the imaginary parts of all four roots of (11) from δ for different values of pump frequency ω and pump

power choosing the dispersion profiles shown in Fig. 1. Typical instability-gain profiles that we have obtained are shown in Fig. 2. We have found that there are two - symmetric with respect to the pump frequency - *pairs* of instability peaks in the spectrum of the perturbation. All these instability peaks are associated with the same root $\kappa = \kappa_{cr}$ of Eq. (11). The regions nearest to the pump frequency can be traced back to the conventional MI, known from the NLSE, and the second peaks are due to the FWM process with far detuned frequencies, as we shall see below.

Condition for both of these instabilities to exist is that the pump frequency should lay between the two ZD points or slightly outside this interval, see Figs. 2 and 3.

In Fig. 2(a,c) the instability gain for our PCF and TF is shown, pumping in anomalous dispersion, with a frequency in between the two ZD points, ω_{ZD1} and ω_{ZD2} . The GVD profiles are also depicted [curve (1)], in order to show that the magnitude of the instability detunings is of the order of the anomalous regime width, $|\omega_{ZD2} - \omega_{ZD1}|$. Moving slightly towards normal dispersion [Fig. 2(b,d)], a gap between the central frequency and MI appears. This has been observed in several numerical simulations, for example in Coen *et al.* [9] and in Dudley *et al.* [10]. However, increasing the pump power one can observe a merging phenomenon between the two kinds of instabilities [curve (3) in Fig. 2], which is even more evident in normal dispersion, due to the fact that in this regime a slight change in the pump frequency towards the deep normal dispersion region corresponds to a large change in the position of MI, while the FWM peaks are almost fixed.

There is a simple theoretical explanation for having instabilities even when $\beta'' > 0$, using the conventional phase matching condition

$$k(\omega + \delta, 2|E_0|^2) + k(\omega - \delta, 2|E_0|^2) - 2k(\omega, |E_0|^2) = 0. \quad (13)$$

Expanding k in Taylor series, knowing that $\beta(\omega) \equiv (\omega/c) \left[1 + \hat{\chi}_{eff}^{(1)}(\omega) \right]^{1/2}$, and considering the detuning δ as a small parameter, one obtains that there is a cancellation between the odd order derivatives in the expansion [21], and it can be easily proved that Eq. (13) can be written as

$$\frac{1}{2}\beta''\delta^2 + \frac{1}{24}\beta''''\delta^4 + \dots \equiv \frac{1}{2} \int_0^\delta [\beta''(\omega + \mu) + \beta''(\omega - \mu)] (\delta - \mu) d\mu = -\bar{\chi}_3|E_0|^2 \quad (14)$$

Even if the pump is injected in a condition of small normal dispersion ($\beta'' > 0$), there can be a contribution due to the even order terms present in Eq.

(14). So in principle the integral in Eq. (14) can be negative, making possible the generation of instability in the normal dispersion regime. This simple analysis of course is valid for small frequency detunings δ , but our equation (11) does not have this limitation.

One point we want to stress is that the dispersion inserted in Eq. (11) has to be considered globally, and not locally, in the sense that for a given pump frequency the entire shape of the GVD curve between and outside the two ZD points has significant influence on the FWM instabilities. Thus, Taylor expansion around a single ZD point is not adequate in this case if one wants to capture all the features of the process.

Finding zeros of the function $\partial_\delta \text{Im}(\kappa_{cr})$, which correspond to the positions of the maximal gains occurring for $\delta = \delta_{cr}$, we calculate a diagram showing frequencies $\omega_{AS,S} = \omega \pm \delta_{cr}$ of the generated waves as functions of ω , see Fig. 3. Fig. 3(a) shows the position of Stokes and anti-Stokes waves for every pump frequency and for three different powers in the case of PCF, while Fig. 3(b) is for our TF. Dashed curves correspond to the two ZD points. It is possible to see the merging process when increasing the pump power (respect to a fixed pump frequency) or moving the pump frequency (respect to fixed pump power).

Note that increasing the power the distance between the MI peaks increases considerably, while the position of FWM peaks remains approximately the same. Moreover, one of the two ZD points (in our case the blue-shifted one) is more "efficient", in the sense that the frequency range excited by the instabilities is larger respect to the other ZD point. An important difference (due to the absence of a Taylor expansion in our equations) between Fig. 3 and other figures present in the literature (for example Ref. [9, 10]) is that our curve is closed, and then the unstable region in the normal dispersion is finite. A simple prediction which follows from this consideration is that it should exist a pump frequency in the normal regime for which all these instabilities are strongly suppressed and completely disappear.

To demonstrate that instabilities found here are essentially FWM instabilities we also show the frequencies of the generated waves calculated using the standard phase matching condition (13). One can see remarkable agreement between results obtained using the exact solution of Eq. (11) and condition (13), confirming the fact that starting with a forward pump wave, we can neglect the influence of the back-propagating wave in the perturbation analysis. Note that the phase matching diagrams presented in [9, 10] in the vicinity of the ZD point with largest frequency capture only a pair of

instability peaks associated with conventional MI.

Existence of the far detuned FWM branches shows that contribution of the FWM processes to the generation of optical supercontinuum can be in some cases even stronger than it has been so far anticipated. Also the initial stage of supercontinuum generation can be attributed to the threshold mechanism of merging between the FWM peaks and the MI peaks [18], clearly visible from Fig. 2 when one increases the pump power. Through this mechanism it is possible to excite all the frequencies between the two FWM peaks, and it may represent an important piece towards the understanding of SCG.

Making qualitative comparison of our results with these experiments is however, complicated by the silica absorption, which is not taken into account in our theory, that is substantial in the far infrared (over 2 microns). Therefore one should expect that far red detuned radiation is strongly absorbed, and this can potentially modify instability conditions and shift the position of the frequencies with maximal gain. Even the Raman effect can affect the instability gain introducing an asymmetry, i.e. a suppression of blue-shifted frequencies respect to the red-shifted ones.

Approximating the propagation constant in Taylor series, one can show that secondary FWM peaks appear in correspondence of the frequency detuning

$$|\delta| \simeq \left(\frac{-12\beta''(\omega)}{\beta''''(\omega)} \right)^{1/2} \quad (15)$$

From Eq. (15) it is evident that the second-order dispersion β'' and the fourth-order dispersion β'''' must have different sign in order to generate the peaks associated to FWM.

Thus pumping the fiber in the region where GVD as function of ω is flatter, i.e. $\beta''''(\omega)$ is smaller, will generate a broader spectrum. In our examples $\beta''''(\omega)$ is smaller near the blue shifted ZD point, therefore pumping in its vicinity one can expect generation of the broadest possible spectrum.

An important estimate, which can be found analytically, is for the critical power required for merging of the MI and FWM peaks. It can be shown that the power required for merging is given by

$$E_m^2 \simeq \frac{6n_{eff}(\omega)c|\beta''(\omega)|^2}{\bar{\chi}_3\omega} \frac{1}{|\beta''''(\omega)|} \quad (16)$$

E_m^2 is less for pump frequencies close to the ZD points. Moreover, because of the factor $1/\omega$ in this relation, E_m^2 is less for the blue-shifted ZD point

respect to the red-shifted one. It follows that in order to improve the width of the generated spectrum one needs to find a compromise between the power required to activate the process, which depends on $|\beta''|^2/|\beta'''|$, and a small value of $|\beta'''|$ at the pump frequency, which regulates the relative distance between the peaks involved in the mechanism. Thus flat and small GVD are the two factors responsible for generation of broad FWM spectrum at low powers, which agrees with experimental finding on generation of optical supercontinuum [8, 9, 10, 11, 16, 19, 26].

The plots of the FWM gain in Fig. 2 are superimposed on the plots showing the dispersion profile of the fiber. It is clear from this figure that dispersion varies quite dramatically through the relevant frequency domain; moreover, the order of magnitude of the detuning relative to the generated frequencies is comparable with the pump frequency itself, such that $|\delta|/\omega$ can not be considered as a small parameter. These are the two reasons which validates the necessity of avoiding Taylor expansion for $\chi^{(1)}$.

CONCLUSIONS

Parametric instabilities in PCFs and TFs have been studied in the context of a general wave equation, avoiding the usual approximations in optics, like the Taylor expansion of the linear susceptibility and the suppression of the contribution of backward waves. Other regions of instability has been found, corresponding to degenerate FWM, which can exist even in a small region of normal dispersion. These peaks of instability are found to be relatively close to the pump frequency in our examples of PCF and TF, but still too far to be detected through ordinary methods of theoretical and numerical analysis. We have evaluated analytically the power required to merge this regions to the modulational instability regions, and we believe that this mechanism (regulated by the usual fourth order dispersion β''' in the language of the ordinary NLSE) can be of fundamental importance in the description of supercontinuum generation in fibers which have a GVD with two zero dispersion points.

ACKNOWLEDGMENTS

We acknowledge J.K. Knight, P.St.J. Russell and T.A. Birks for several useful discussions.

References

- [1] R.H. Stolen, and G.D. Bjorkholm, IEEE J. Quantum Electron. **18**, 1062 (1982).
- [2] O. Aso, M. Tadakuma, and S. Namiki, Furukawa Rev. **19**, 63 (2000).
- [3] G.P. Agrawal, *Nonlinear Fiber Optics* (Academic Press, San Diego, 2001).
- [4] W. Washio, K. Inoue, and S. Kishida, Electron. Lett. **16**, 658 (1980).
- [5] D.K. Serkland and P. Kumar, Opt. Lett. **24**, 92 (1999).
- [6] R.H. Stolen, M.A. Bosch, and C. Lin, Opt. Lett. **6**, 213 (1981).
- [7] J.C. Knight, T.A. Birks, P.St.J. Russell, and D.M. Atkin, Opt. Lett. **21**, 1547 (1996).
- [8] T.A. Birks, W.J. Wadsworth, and P.St.J. Russell, Opt. Lett. **25**, 1415 (2000).
- [9] S. Coen, A.H.L. Chau, R. Leonhardt, J.D. Harvey, J.C. Knight, W.J. Wadsworth, and P.St.J. Russell, J. Opt. Soc. Am. B **19**, 753 (2002).
- [10] J.M. Dudley, L. Provino, N. Grossard, H. Maillotte, R.S. Windeler, B.J. Eggleton, and S. Coen, J. Opt. Soc. Am. B **19**, 765 (2002).
- [11] J.E. Sharping, M. Fiorentino, A. Coker, P. Kumar, and R.S. Windeler, Opt. Lett. **26**, 1048 (2001).
- [12] A.M. Zheltikov, Physics Uspekhi **43**, 1125 (2000).
- [13] J. Broeng, D. Mogilevstev, S.E. Barkou, and A. Bjarklev, Opt. Fiber Tech. **5**, 305 (1999).
- [14] A.W. Snyder, and J.D. Love, *Optical Waveguide Theory* (Chapman and Hall, London, 1983).
- [15] J.C. Knight, T.A. Birks, P.St.J. Russell, and J.P. de Sandro, J. Opt. Soc. Am. A, **15**, 748 (1998).

- [16] A. Ortigosa-Blanch, J.C. Knight, and P.St.J. Russell, *J. Opt. Soc. Am. B* (2002, to be published).
- [17] W.J. Wadsworth, A. Ortigosa-Blanch, J.C. Knight, T.A. Birks, T.P.M. Man, and P.St.J. Russell, *J. Opt. Soc. Am. B*, **19**, 2148 (2002).
- [18] A.V. Husakou, and J. Herrmann, *J. Opt. Soc. Am. B* **19**, 2171 (2002).
- [19] G. Millot, A. Sauter, J.M. Dudley, *Opt. Lett.* **27**, 695 (2002).
- [20] S. Song, C.T. Allen, K.R. Demarest, and R. Hui, *IEEE J. Light. Tech.* **17**, 2285 (1999).
- [21] M.J. Potasek, *Opt. Lett.* **12**, 921 (1987).
- [22] K.J. Blow, D. Wood, *IEEE J. Quantum Electron.* **25**, 2665 (1989).
- [23] M. Yu, C.J. McKinstrie, and G.P. Agrawal, *Phys. Rev. E* **52**, 1072. (1995).
- [24] E.A. Golovchenko, and A.N. Pilipetskii, *J. Opt. Soc. Am. B* **11**, 92 (1994).
- [25] A.V. Husakou, and J. Herrmann, *Phys. Rev. Lett.* **87**, 203901 (2001).
- [26] J. Herrmann, U. Griebner, N. Zhavoronkov, A. Husakou, D. Nickel, J.C. Knight, W.J. Wadsworth, P.St.J. Russell, and G. Korn, *Phys. Rev. Lett.* **88**, 173901 (2002).

List of figures

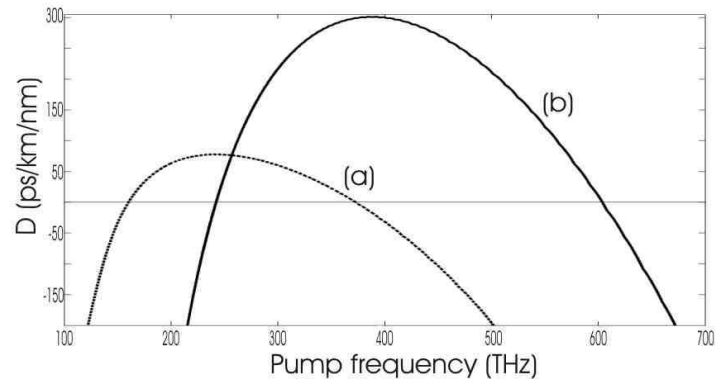


Figure 1: Group-velocity dispersion (GVD) for our examples of PCF (a) and TF (b) described in the text.

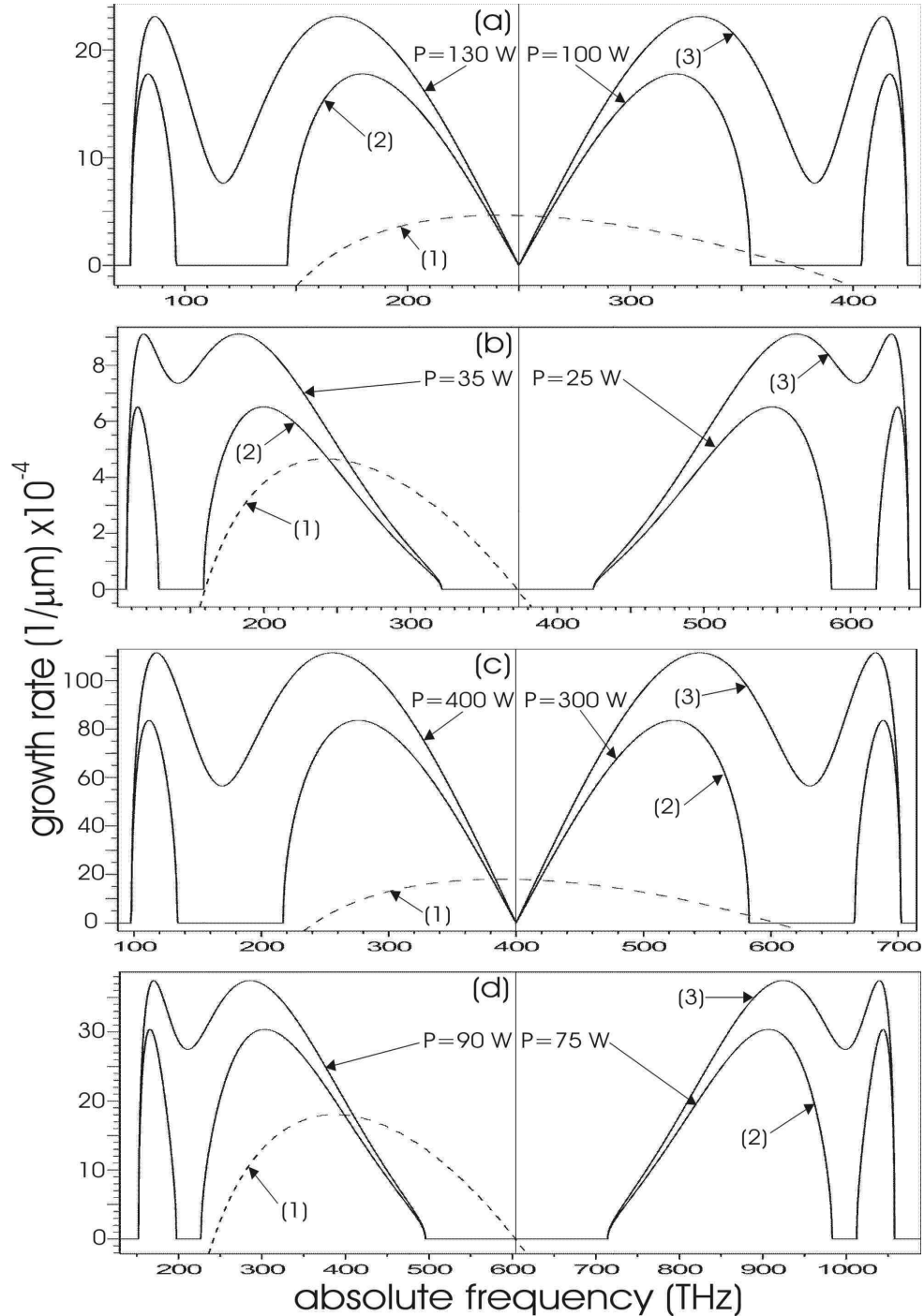


Figure 2: Curves (1) show the dependence of the rescaled parameter $D(\omega)$ on frequency for the chosen PCF and TF with $1 \mu\text{m}$ core diameter. To get physical values of D one needs to multiply the values for the instability gain by the factor 17 ps/nm/km . Curves (2) and (3) show the dependence of the instability gain $\text{Im}(\kappa_{cr})$ for PCF (a,b) and TF (c,d) on frequency for different pump powers $P = |E_0|^2$. (2) is for $|E_0|^2 < |E_m|^2$ and (3) is for $|E_0|^2 > |E_m|^2$. The central frequency in every picture corresponds to the pump frequency.

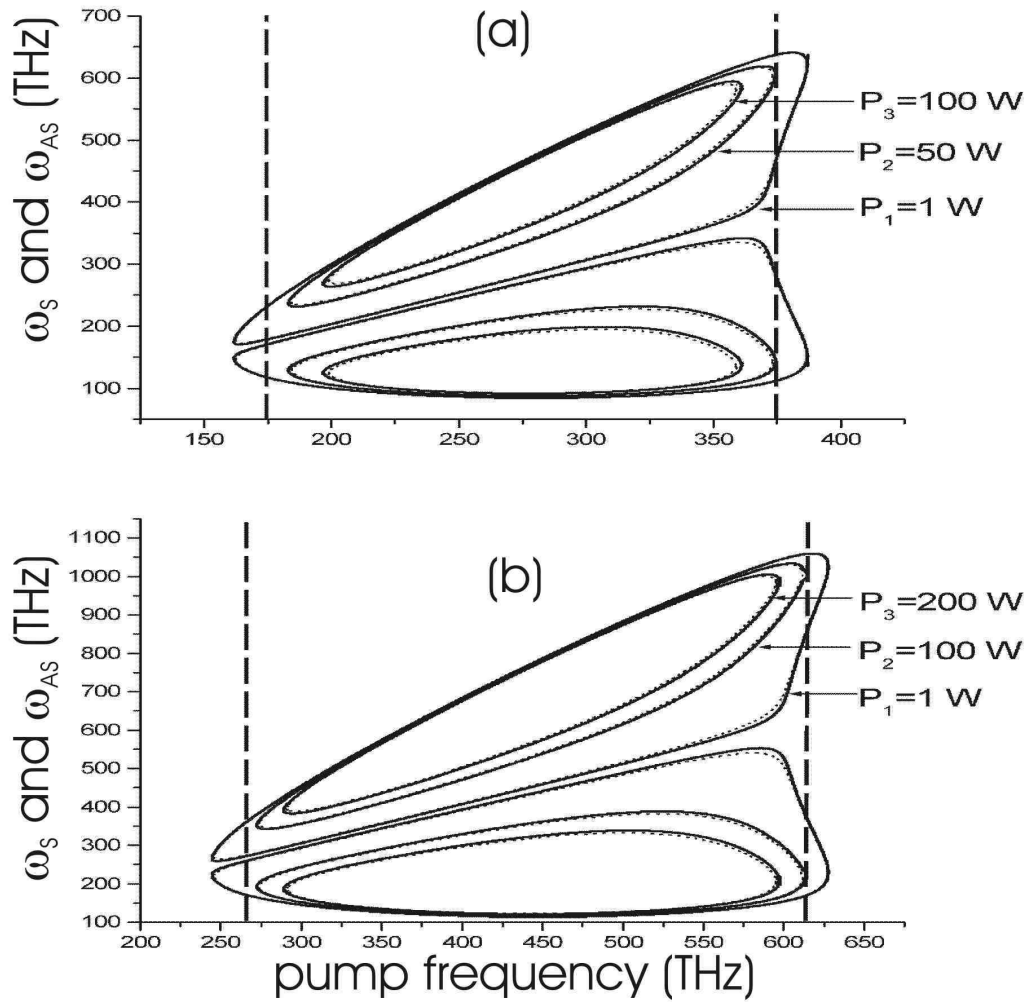


Figure 3: Diagrams showing positions of the maximal instability gain vs pump frequency calculated from Eq. (7) for different powers $P = |E_0|^2$ in PCF (a) and TF (b). Dots show the same values calculated using phase matching condition (8). ZD points are indicated by dashed vertical lines.